Meteorologische Zeitschrift, Vol. **15**, No. 6, 611-624 (December 2006)

A model of dust transport applied to the Dead Sea Area

BERNHARD VOGEL*, CORINNA HOOSE[1], HEIKE VOGEL and CHRISTOPH KOTTMEIER

Institut für Meteorologie und Klimaforschung, Forschungszentrum Karlsruhe/Universität Karlsruhe, Karlsruhe, Germany
[1]current affiliation: Institut für Atmosphäre und Klima, ETH Zürich, Switzerland

(Manuscript received December 1, 2005; in revised form May 5, 2006; accepted July 20, 2006)

Abstract

We applied a parameterization for the emission of mineral dust particles which takes into account the relevant processes such as saltation and combines previous, physically based parameterizations. The size distribution of the soil particles is taken into account to describe the saltation. The emitted particles are described by three log-normal distributions with fixed standard deviations. A comparison of the results of a stand alone version of our parameterization with observations shows that despite tuning of model parameters there are still differences. Finally, we included the parameterization within our three-dimensional mesoscale model system for the area of the Dead Sea. The channelling effect of the Jordan Valley and stable stratification during the day modifies the horizontal distribution of the dust particles. At greater distances the size and the mass distributions of the particles is shifted towards smaller diameters due to sedimentation which is important for radiative feedback mechanisms. Sensitivity runs show the advantage of the parameterization which allows a time dependent ratio of the saltation and the emission flux at each grid point.

Zusammenfassung

Wir haben zwei bereits vorhandene physikalische Parametrisierungen zur Beschreibung der Emission von Mineralstaub kombiniert. Bei der Beschreibung der Saltation wird die Größenverteilung der am Boden liegenden Partikel berücksichtigt. Dies geschieht unter Verwendung dreier Moden. Die emittierten und dem atmosphärischen Transport unterliegenden Partikel werden ebenfalls mittels dreier Log-Normal Verteilungen beschrieben. Ein Vergleich von berechneten und gemessenen Saltations- und Emissionsflüssen, die mit einer "stand alone" Version der Parametrisierung durchgeführt wurde, zeigt dass in einzelnen Fällen noch immer größere Abweichungen bestehen. Schließlich haben wir die neue Parametrisierung in ein dreidimensionales Strömungs- und Ausbreitungsmodell integriert und das so erweiterte Modell auf das Gebiet des Toten Meeres angewendet. Es zeigt sich, dass der Kanalisierungseffekt des Jordantales und die im Bereich des Toten Meeres auch tagsüber auftretenden stabilen Schichtungsverhältnisse zu einer Modifikation der Konzentrationsverteilungen führt. Mit größer werdendem Abstand von der Quellregion verschieben sich auf Grund der Sedimentation die Größenverteilungen zu kleineren Radien hin. Diese Modifikation der Größenverteilungen gilt es richtig zu beschreiben, wenn die Wechselwirkung mit der Strahlung quantifiziert werden soll. Sensitivitätsuntersuchungen zeigen den Vorteil unserer Parametrisierung, die ein zeitlich variables Verhältnis zwischen Saltations- und Emissionsfluss an jedem Gitterpunkt zulässt.

1 Introduction

Mineral dust particles are lifted into the atmosphere in a great amount during impressive dust storm events. Besides sea salt mineral dust is the most important source of aerosol mass for the atmosphere (SEINFELD and PANDIS, 1998). Not only natural but also human activities as farming, stone crushing, transportation, and desertification due to anthropogenic climate change can contribute to the emissions of mineral dust. In the source areas wind erosion often causes a loss of agricultural soil, while in other areas (e.g. the big cities in East Asia) high dust loads are leading to a remarkable reduction of visibility. The deposition of mineral dust in the oceans leads to an impact on the ecosystem (BISHOP et al. 2002). Microorganisms can be transported on mineral dust particles over long distances (GRIFFIN et al., 2003). Airborne mineral dust particles are found in a size range of 0.1 to 50 μm. Those particles have a mean lifetime of 3 to 7 days (ZENDER et al. 2004). Therefore, the spatial and temporal distribution is very inhomogeneous. Important source areas for mineral dust are the Sahara especially the Bodele Depression in Chad, the Gobi and Takla-Makan desert in Asia (SHAO, 2000).

Mineral dust particles have an influence on the radiation budget of the earth not only on the global scale but also locally (direct effect). However, this impact is not quantified yet. Depending on the size distribution and the chemical composition mineral dust scatters and absorbs both infrared and shortwave radiation. The scattering in the shortwave range leads to a cooling of the atmosphere while the absorption in the long wave range

*Corresponding author: Bernhard Vogel, Institut für Meteorologie und Klimaforschung, Forschungszentrum Karlsruhe/Universität Karlsruhe, Postfach 3640, 76021 Karlsruhe, Germany, e-mail: bernhard.vogel@imk.fzk.de

DOI: 10.1127/0941-2948/2006/0168

Gebrüder Borntraeger Stuttgart, Germany

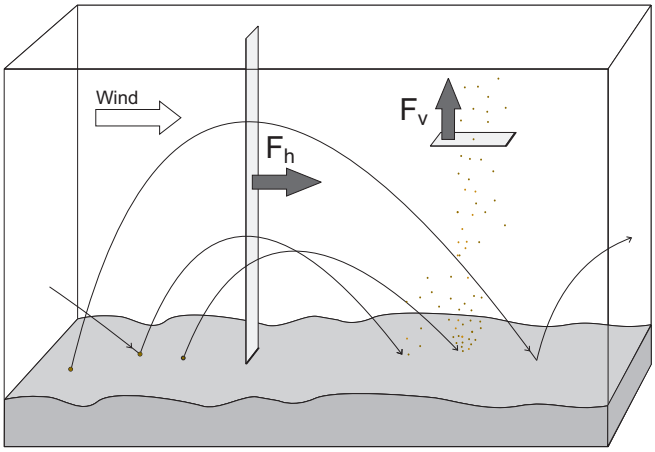

Figure 1: Illustration of the vertically integrated horizontal flux of saltation particles F_h and the vertical flux of emitted dust particles F_v.

leads to an increase of the greenhouse effect (ANDREAE, 1996). However, the modelled quantitative effect of mineral dust on the global scale depends strongly on the assumptions made for the particles (TEGEN, 2003).

Mineral dust has an impact on cloud formation (indirect effects). However, there is no clear picture at the moment. While ROSENFELD et al. (2001) suggested a positive feedback to desertification MILLER et al. (2004) found a negative one. LEVIN et al. (1996) studied the effect of desert particles coated with sulphate on rain formation. They found that this coating converts the dust particles into giant cloud condensation nuclei.

In order to describe the spatial and temporal distribution of mineral dust particles it is necessary to describe the source term in an accurate way. This has to be done in a parameterized form and is the most crucial point in mineral dust modelling. Airborne mineral dust particles are not lifted directly into the atmosphere by the Bernoulli effect, since the binding energies due to Coulomb forces are too high. Instead, they are brought into the atmosphere by the so called saltation process. Particles with a diameter larger than approximately 50 μm, which can be lifted into the atmosphere due to the Bernoulli effect but fall rapidly back down to the surface due to gravitational forces, release smaller particles which have a small settling velocity and therefore can remain in the atmosphere. For example, measurements of the horizontal sand transport in the atmospheric surface layer have been reported by SCHÖNFELDT and VON LOEWIS (2003). They measured count rates of a saltiphone and tried to quantify the sand transport in response to shear stress and wind speed fluctuations. Further, the threshold velocity for the initiation of the saltation process was measured (SCHÖNFELDT, 2004).

BAGNOLD (1941) derived a first theoretical framework for the treatment of emissions of mineral dust. Further theories were developed by e. g. OWEN (1964) and WHITE (1979). GREELEY and IVERSEN (1985) and SHAO (2000) give an overview on individual theories on saltation, dust emission and dust dispersion. In general one has to distinguish between two particle fluxes. The first is the horizontal saltation flux of larger particles close to the surface; the second one is the vertical emission flux of the smaller size particles which is the source term for atmospheric modelling (see Figure 1).

The first numerical models that treated the dust transport on the regional and global scale did not explicitly account for the saltation process. Instead they used a parameterization where the vertical emission flux depends directly on the friction velocity or on the wind speed close to the surface. Examples for those models are described in GILLETTE and PASSI (1988); GENTHON (1992); TEGEN and FUNG (1994); GINOUX et al. (2001), and IN and PARK (2002).

A more detailed description of the mineral dust emissions was introduced by the work of MARTICORENA and BERGAMETTI (1995). They included an explicit diameter-dependent parameterization of the saltation flux. The vertical emission flux is then assumed proportional to the saltation flux. The improvement of the description of these processes is connected with the necessity of additional input parameters as the size distribution of the particles at the ground. Further model applications that took into account saltation and vertical emission fluxes are those of MARTICORENA et al. (1997), LU and SHAO (1999, 2001), SHAO and LU (2000), and NICKOVIC et al. (2001). However, these studies did not take into account the size distribution of the emitted particles. The dependence of the size of the vertically emitted particles on the size of the saltation particles was taken into account by SHAO (2001) and ALFARO and GOMES (2001) who made individual assumptions for the size-dependent relation between the saltation and the vertical emission flux instead of a simple proportionality. Both formulations were applied in model simulations by GONG et al. (2003), GRINI and ZENDER (2004), and SONG (2004).

Most of the previous model applications were performed on the global or the hemispheric scale. Since the direct input of the mineral dust particles happens on the regional scale and below, we used the non-hydrostatic mesoscale model system KAMM/DRAIS (VOGEL et al. 1995; RIEMER et al., 2003) to calculate the atmospheric variables and the transport of mineral dust. Based on the work of SHAO (2001) and ALFARO and GOMES (2001) we combined two parameterizations of the threshold friction velocity and the vertical flux of mineral dust to a new microphysically detailed parameterization for the emission of mineral dust as will be outlined in section 3. We will compare this parameterization in a stand alone version with available observations. The parameterization of the mineral dust emission

was included in the modal aerosol model MADEsoot (RIEMER et al., 2003) which is based on the work of ACKERMANN et al. (1998) and SCHELL et al. (2001). We then coupled this improved aerosol model (MADEdust) with the three-dimensional version of the model system KAMM/DRAIS in an online mode that means all processes were treated at the same time by the model. KAMM/DRAIS/MADEdust was then applied for the greater area of the Dead Sea to treat mineral dust transport which origins from the Negev desert. Unfortunately, the lack of the necessary input parameters for the source parameterization for this region represents a major uncertainty.

2 The regional scale model system

According to MADEsoot we are using the modal approach to describe the dispersion of the mineral dust particles. Following ALFARO and GOMES (2001) we are using three modes.

The following equations describe the transport and the diffusion of mineral dust particles:

$$\begin{aligned}\frac{\partial \overline{N_i}}{\partial t} &= -\bar{u}\cdot\frac{\partial \overline{N_i}}{\partial x} - \bar{v}\cdot\frac{\partial \overline{N_i}}{\partial y} - \bar{w}\cdot\frac{\partial \overline{N_i}}{\partial z} \\ &\quad + \frac{\partial}{\partial x}\left(Kh_{xx}\cdot\frac{\partial \overline{N_i}}{\partial x}\right) + \frac{\partial}{\partial y}\left(Kh_{yy}\cdot\frac{\partial \overline{N_i}}{\partial y}\right) \\ &\quad + \frac{\partial}{\partial z}\left(Kh_{zz}\cdot\frac{\partial \overline{N_i}}{\partial z}\right) - \frac{\partial v_{sN,i}\cdot\overline{N_i}}{\partial z} + E_{N,i} \quad i = 1,3\end{aligned} \tag{2.1}$$

$$\begin{aligned}\frac{\partial \overline{m_i}}{\partial t} &= -\bar{u}\cdot\frac{\partial \overline{m_i}}{\partial x} - \bar{v}\cdot\frac{\partial \overline{m_i}}{\partial y} - \bar{w}\cdot\frac{\partial \overline{m_i}}{\partial z} \\ &\quad + \frac{\partial}{\partial x}\left(Kh_{xx}\cdot\frac{\partial \overline{m_i}}{\partial x}\right) + \frac{\partial}{\partial y}\left(Kh_{yy}\cdot\frac{\partial \overline{m_i}}{\partial y}\right) \\ &\quad + \frac{\partial}{\partial z}\left(Kh_{zz}\cdot\frac{\partial \overline{m_i}}{\partial z}\right) - \frac{\partial v_{sm,i}\cdot\overline{m_i}}{\partial z} + E_{m,i} \quad i = 1,3\end{aligned} \tag{2.2}$$

The index i refers to the different modes. $\overline{N_i}$ and $\overline{m_i}$ are the Reynolds averaged number density and the Reynolds averaged mass density, respectively. $\bar{u}$, $\bar{v}$, and $\bar{w}$ are the components of the wind velocity. It is assumed that the turbulent exchange coefficient for heat Kh that is taken from the meteorological part of the model is identical to those of number and mass density. $v_{sN,i}$ and $v_{sm,i}$ are the sedimentation velocities for number and mass density. $E_{N,i}$ and $E_{m,i}$ are the temporal changes of number and mass densities due to emissions. In case of the mineral dust $E_{N,i}$ and $E_{m,i}$ are greater than zero only at the surface.

All equations are transformed into a terrain following coordinate system.

The number and mass distributions are assumed to be log-normal distributions. The number distribution is given by

$$n_i(\ln d_p) = \frac{\bar{N_i}}{\sqrt{2\cdot\pi}\cdot\ln\sigma_i}\cdot\exp\left(-\frac{(\ln d_p - \ln d_{g,i})^2}{2\cdot\ln^2\sigma_i}\right) \quad i = 1,3 \tag{2.3}$$

with the diameter d_p, the number median diameter $d_{g,i}$, and the geometric standard deviation σ_i. The latter is assumed to be constant for each mode.

The corresponding equation for the mass distribution reads as:

$$m_i^*(\ln d_p) = \frac{\bar{m_i}}{\sqrt{2\cdot\pi}\cdot\ln\sigma_i}\cdot\exp\left(-\frac{(\ln d_p - \ln d_{g3,i})^2}{2\cdot\ln^2\sigma_i}\right) \quad i = 1,3 \tag{2.4}$$

$d_{g3,i}$ is the mass median diameter. $d_{g,i}$ and $d_{g3,i}$ are related by $d_{g,i} = d_{g3,i}\cdot\exp(-3\cdot\ln^2\sigma_i)$. The median diameter of the log normal distributions can vary with time and space and is determined from:

$$d_{g,i} = \sqrt[3]{\frac{\overline{m_i}}{\frac{\pi}{6}\cdot\rho_p\cdot\exp\left(\frac{9}{2}\cdot\ln^2\sigma_i\right)\cdot\overline{N_i}}} \quad i = 1,3 \tag{2.5}$$

ρ_p is the bulk density of the particles.

The sedimentation velocities for the number and the mass density are given by Stokes Law with Cunningham slip correction, integrated over the log-normal distribution (BINKOWSKI and SHANKAR, 1995, and references therein):

$$v_{sN,i} = \frac{g\cdot\rho_p}{18\cdot\nu\cdot\rho_a}\cdot\left[\exp\left(2\cdot\ln^2\sigma_i\right) + 1.246\cdot\frac{2\cdot\lambda_a}{d_{g,i}}\cdot\exp\left(\frac{1}{2}\cdot\ln^2\sigma_i\right)\right] \tag{2.6}$$

$$v_{sm,i} = \frac{g\cdot\rho_p}{18\cdot\nu\cdot\rho_a}\cdot\left[\exp\left(8\cdot\ln^2\sigma_i\right) + 1.246\cdot\frac{2\cdot\lambda_a}{d_{g,i}}\cdot\exp\left(\frac{7}{2}\cdot\ln^2\sigma_i\right)\right] \tag{2.7}$$

$d_{g,i}$ is determined from equation (2.5). ρ_a is the air density, g the acceleration of gravity, ν the kinematical viscosity of air, and λ_a mean free path of air.

3 Parameterization of the emission

In order to calculate the emission of dust particles it is necessary to calculate two individual fluxes namely the vertically integrated flux of saltation particles parallel to

the surface F_{th} (in kg m^{-1} s^{-1}) and the vertical flux of smaller particles injected into the atmosphere F_{tv} (in kg m^{-2} s^{-1}). For an illustration see Figure 1. In the following the vertically integrated flux of saltation particles parallel to the surface is named horizontal saltation flux.

The source term of mode i in equation (2.2) is then given by the divergence of the vertical mass flux $F_{tv,i}$, calculated on the numerical grid.

$$E_{m,i} = -\frac{\partial F_{tv,i}}{\partial z} \approx \frac{F_{tv,i}}{\Delta z_s} \quad i = 1,3 \tag{3.1}$$

Δz_s is the thickness of the lowest model layer above the surface. The corresponding source term for the particle number concentration is given by:

$$E_{N,i} = \frac{6}{\pi \cdot \rho_p \cdot d_{d,i}^3} \cdot \exp\left(-\frac{9}{2} \cdot \ln^2 \sigma_i\right) \cdot E_{m,i} \quad i = 1,3 \tag{3.2}$$

$d_{d,i}$ is the initial mass median diameter at the source.

3.1 Calculation of the horizontal saltation flux

The onset of the saltation process can be parameterized by a size-dependent threshold value $u_{*t}(d_p)$ of the friction velocity u_*. For ideal (smooth and dry) conditions SHAO and LU (2000) derived

$$u_{*ts}(d_p) = \sqrt{A_n \cdot \left(\frac{\rho_p}{\rho_a} \cdot g \cdot d_p + \frac{\gamma}{\rho_a \cdot d_p}\right)} \tag{3.3}$$

with the empirically determined parameters $A_n = 0.0123$ and $\gamma = 3 \cdot 10^{-4}$ kg s^{-2}.

For non-ideal conditions, $u_{*ts}(d_p)$ has to be modified in order to account for varying soil roughness and humidity. In a simplistic approach, it is modified by two factors, f_{z0} and f_η:

$$u_{*t}(d_p) = \frac{f_\eta \cdot u_{*ts}(d_p)}{f_{z_0}} \tag{3.4}$$

For the influence of varying soil roughness on the threshold friction velocity, we use an empirical relation by ALFARO and GOMES (1995).

$$f_{z_0} = 1 - 0.55 \cdot (z_0)^{0.4} \cdot \ln\left(\frac{z_0}{z_{0s}}\right) \tag{3.5}$$

z_0 is the roughness length in mm. The roughness length for smooth conditions, z_{0s} , is approximated by 1/30 of the diameter of the biggest soil particles (in mm). Soil humidity also increases $u_{*t}(d_p)$. FECAN et al. (1999) derived the following expression:

$$f_\eta = \sqrt{1 + 1.21 \cdot (\eta - \eta')^{0.68}} \tag{3.6}$$

for $\eta > \eta'$ and 1 elsewhere.
η denotes the gravimetric soil water content in %, η' the minimal value of η which is related to soil clay content: $\eta' = 0.0014 \cdot (\%\ \text{clay})^2 + 0.17 \cdot (\%\ \text{clay})$. In this study we assumed $f_\eta = 1$ for all cases i.e. $\eta' = \eta$.

The horizontal saltation flux $F_h(d_p)$ of particles with diameter d_p is now parameterized as follows (WHITE, 1979):

$$F_h(d_p) = C \cdot \frac{\rho_a}{g} \cdot u_*^3 \cdot \left(1 + \frac{u_{*t}(d_p)}{u_*}\right) \cdot \left(1 - \frac{u_{*t}^2(d_p)}{u_*^2}\right) \tag{3.7}$$

F_h is to be interpreted as the vertically integrated horizontal saltation flux. This makes sense since after a short time all saltation particles return to the earth's surface. The corresponding unit of F_h is kg m^{-1} s^{-1}. For illustration see Figure 1.

Under idealized conditions, the constant C has a value of 2.61. To match field measurements of F_h, C has to be adjusted to much lower values (GOMES et al., 2003). For the total saltation flux, equation (3.7) has to be integrated over all saltation particle sizes, weighted with their cross sectional area and the size distribution of the soil particles, $n_s(\ln d_p)$.

$$F_{th} = \int_{-\infty}^{\infty} F_h(d_p) \cdot \frac{\frac{\pi}{4} \cdot d_p^2 \cdot n_s(\ln d_p)}{\int_{-\infty}^{\infty} \frac{\pi}{4} \cdot d_p^2 \cdot n_s(\ln d_p)\ d \ln d_p} d \ln d_p \tag{3.8}$$

The size distribution of the number density of the soil particles is replaced by the size distribution of the mass density applying the following relation:

$$n_s(\ln d_p) = m_s^*(\ln d_p) \cdot \frac{6}{\pi \cdot \rho_p \cdot d_p^3} \tag{3.9}$$

In addition we assume that the size distribution m_s^* is the sum of up to three log-normal distributions:

$$m_s^*(\ln d_p) = \sum_{j=1}^{3} m_{s,j}^*(\ln d_p) \tag{3.10}$$

with

$$m_{s,j}^*(\ln d_p) = \frac{a_j \cdot m_s}{\sqrt{2 \cdot \pi} \cdot \ln \sigma_{s,j}} \cdot \exp\left(-\frac{(\ln d_p - \ln d_{gms,j})^2}{2 \cdot \ln^2 \sigma_{s,j}}\right) \quad j = 1,3 \tag{3.11}$$

m_s is the total mass density of all dust particles at the surface. a_j is the mass fraction, $\sigma_{s,j}$ the geometric deviation, and $d_{gms,j}$ the mass median diameter of mode j.

Table 1: Properties of the three dust modes (ALFARO and GOMES, 2001).

	Mode 1	**Mode 2**	**Mode 3**
$d_{g3,i}$ in µm	1.5	6.7	14.2
σ_i	1.7	1.6	1.5
e_i in g cm^{-2} s^{-2}	3.61	3.52	3.46

3.2 Calculation of the vertical dust flux

For the calculation of the vertical dust flux F_{tv}, we follow the approach of ALFARO and GOMES (2001) basing on partitioning of the available kinetic energy into the three dust modes. The vertical mass flux of dust mode i, released by saltation particles of diameter d_p, is given by:

$$F_{v,i}(d_p) = \frac{\pi}{6} \cdot \rho_p \cdot d_{d,i}^3 \cdot \frac{p_i(d_p) \cdot E(d_p)}{e_i} \tag{3.12}$$

$E(d_p)$ denotes the kinetic energy flux of saltation particles with diameter d_p and is approximately proportional to the horizontal saltation flux:

$$E(d_p) = \beta \cdot F_h(d_p) \tag{3.13}$$

with $\beta = 163$ m s^{-2}. e_i is the binding energy of mode i, $d_{d,i}$ its mass median diameter. $p_i(d_p)$ is the fraction of $E(d_p)$ that is available to release particles of mode i. The dimensionless functions $p_i(d_p)$ have been determined by ALFARO and GOMES (2001) with the following assumptions. The mean kinetic energy of the saltation particles with diameter d_p is given by:

$$e_k(d_p) = \frac{\pi}{12} \cdot \rho_p \cdot d_p^3 \cdot (17 \cdot u_*)^2 \tag{3.14}$$

$p_i(d_p)$ depends on $e_k(d_p)$ and on the binding energies e_i. These energies are assumed to have a constant value for each of the three dust modes, as listed in Table 1. The smallest mode has the highest binding energy. Particles of mode i can be emitted only when $e_k(d_p) \geqslant e_i$, and the higher $e_k(d_p)$, the larger the fraction available to release the finest dust particles. The functions p_i as determined by ALFARO and GOMES (2001) are listed in Table 2.

For the total vertical dust fluxes, equation (3.12) has to be integrated over all saltation particle sizes, weighted with their cross sectional area and the size distribution of the soil particles, $n_s(\ln d_p)$:

$$F_{tv,i} = \int_{-\infty}^{\infty} F_{v,i}(d_p) \cdot \frac{\frac{\pi}{4} \cdot d_p^2 \cdot n_s(\ln d_p)}{\int_{-\infty}^{\infty} \frac{\pi}{4} \cdot d_p^2 \cdot n_s(\ln d_p)\, d\ln d_p} \, d\ln d_p \tag{3.15}$$

Applying equation (3.9) in (3.15) results in:

$$F_{tv,i} = \int_{-\infty}^{\infty} F_{v,i}(d_p) \cdot \frac{1}{d_p} \cdot \frac{m_s^*(\ln d_p)}{\int_{-\infty}^{\infty} \frac{1}{d_p} m_s^*(\ln d_p)\, d\ln d_p} \, d\ln d_p \qquad i = 1,3. \tag{3.16}$$

The final equation of the vertical dust flux for the three modes then reads as:

$$F_{tv,i} = \int_{-\infty}^{\infty} F_{v,i}(d_p) \cdot \frac{1}{d_p} \cdot \frac{\sum_{j=1}^{3} \frac{a_j}{\ln \sigma_{s,j}} \cdot \exp\left(-\frac{\left(\ln d_p - \ln d_{gms,j}\right)^2}{2 \cdot \ln^2 \sigma_{s,j}}\right)}{\int_{-\infty}^{\infty} \frac{1}{d_p} \cdot \sum_{j=1}^{3} \frac{a_j}{\ln \sigma_{s,j}} \cdot \exp\left(-\frac{\left(\ln d_p - \ln d_{gms,j}\right)^2}{2 \cdot \ln^2 \sigma_{s,j}}\right) d\ln d_p} \, d\ln d_p \qquad i = 1,3 \tag{3.17}$$

It is impossible to solve this integral analytically. For the numerical integration the integral is split up into intervals of $\ln d_p$. Below a certain diameter, $p_i(d_p)$ and therefore the integrand equals zero. In order to optimize the calculation of this integral, summation starts at the diameter where the integrand first assumes a positive value and the first interval of $\ln d_p$ is not fixed but varies in function of u_*. For the remaining range of $\ln d_p$ a relatively small number of intervals is then sufficient.

For discussion in section 3.3, the saltation and vertical emission fluxes are summed up over the three modes:

$$F_{th} = \sum_{i=1}^{3} F_{th,i} \tag{3.18}$$

$$F_{tv} = \sum_{i=1}^{3} F_{tv,i} \tag{3.19}$$

The essence of this parameterization is as follows: F_{th} is driven by the friction velocity u_*, whereas F_{tv} is driven by F_{th}. It is only F_{tv} that enters, in form of its vertical divergence, equation (2.1) and (2.2) as emission in the lowest layer.

3.3 Comparison with observations

As a next step we compare the results of our parameterization with observations in a stand alone version. GOMES et al. (2003) carried out measurements in Spain and in Niger. They measured u_*, z_0, F_{th}, and F_{tv}. Eleven data sets are available for Spain and 31 for Niger, respectively. Since the humidity at the surface and in the soil was not measured we assumed $f_\eta = 1$. For the particle bulk density, we always assume $\rho_p = 2.65$ g cm^{-3}. The vertically integrated horizontal saltation flux, averaged

Table 2: The partitioning functions p_i (ALFARO and GOMES, 2001).

	p_1	p_2	p_3
$e_k(d_p) < e_3$	0	0	0
$e_3 \le e_k(d_p) < e_2$	0	0	1
$e_2 \le e_k(d_p) < e_1$	0	$\frac{e_k(d_p) - e_2}{e_k(d_p) - e_3}$	$1 - p_2$
$e_1 \le e_k(d_p)$	$\frac{e_k(d_p) - e_1}{e_k(d_p) - e_3}$	$\left(1 - \frac{e_k(d_p) - e_1}{e_k(d_p) - e_3}\right) \cdot \frac{e_k(d_p) - e_2}{e_k(d_p) - e_3}$	$1 - p_1 - p_2$

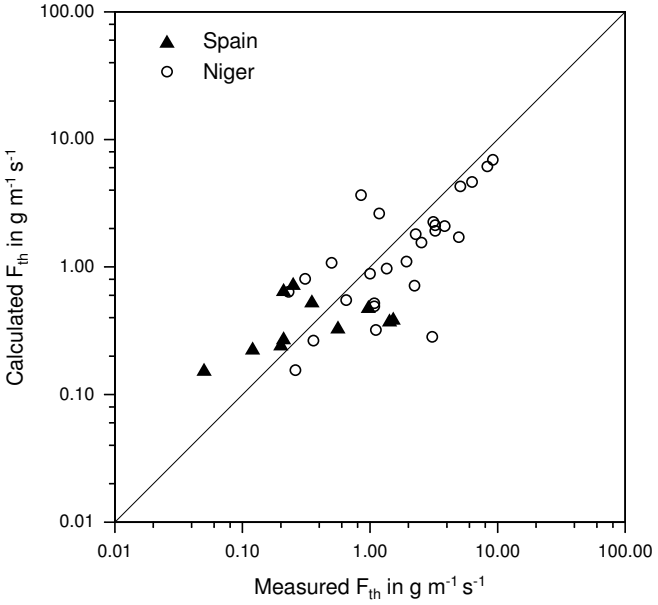

Figure 2: Measured and calculated F_{th} for two sites.

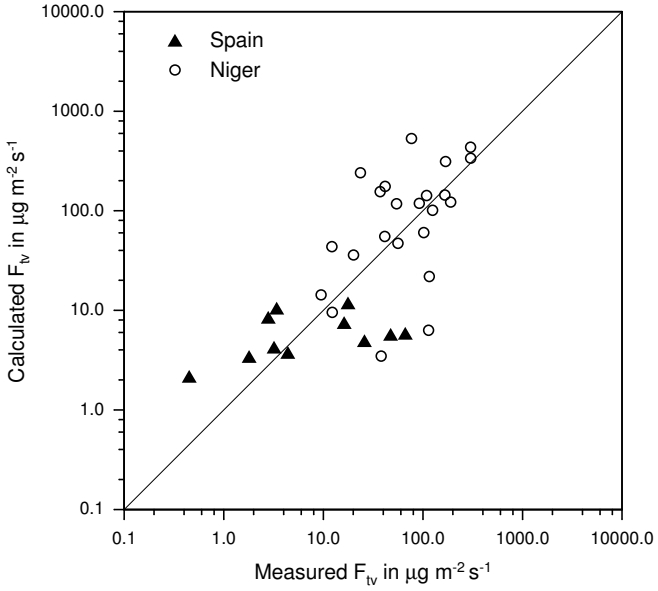

Figure 3: Measured and calculated F_{tv} for two sites.

over the particle diameters, has been given in equation (3.8). In order to calculate this formula the parameters in equation (3.11) have to be specified. These parameters were measured by GOMES et al. (2003) and are given in Table 3. Finally we used C (equation 3.7) as a tuning parameter.

Figure 2 shows computed versus observed values of F_{th}. We used $C = 0.02$ in case of Spain and $C = 1$ for Niger for maximum agreement between observed and simulated saltation flux. This is in agreement with the results of GOMES et al. (2003) who used the parameterization by ALFARO and GOMES (2001). This parameterization and ours differ with respect to the calculation of u_{*ts} where ours is an extension. GOMES et al. (2003) suggest that small values of the parameter C are related to crusting of the soil and to limited supply of loose particles. The differences between simulated and measured fluxes are similar to those of GOMES et al. (2003). In most cases the differences are less than a factor of 3 but for individual cases differences up to a factor of 10 are found. This shows that there is still the necessity of improvement of the parameterization which requires additional measurements.

Figure 2 shows that in the case of Spain the scatter is larger than in the case of Niger. Similar u_* and z_0 values coincided with large differences in the saltation flux. GOMES et al. (2003) relate this to supply limitation, i. e. the fact that at the beginning of a dust event there is looser material available at the surface than later on. This effect is not covered by our parameterization but will be taken into account by future improvements.

Finally, we compared the measured vertical dust flux F_{tv} values with the results of our parameterization (equa-

Table 3: Parameters of the soil particle size distribution for two individual soils (GOMES et al., 2003).

	Spain			**Niger**	
	Mode 1	Mode 2	Mode 3	Mode 1	Mode 2
$d_{gms,j}$ in µm	115	280	529	160	372
$\sigma_{s,j}$	1.8	1.5	1.2	1.9	1.5
a_j	0.46	0.32	0.22	0.44	0.56

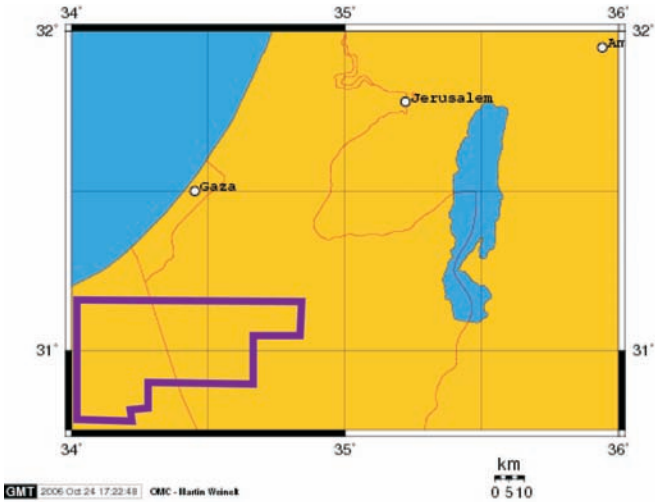

Figure 4: Model domain. The thick line indicates the area where emissions of dust are allowed.

Table 4: Parameters of the soil particle size distribution for a typical Saharan soil (from CHATENET et al., 1996).

	Mode 1	**Mode 2**
$d_{gms,j}$ in µm	210	690
$\sigma_{s,j}$	1.6	1.6
a_j	0.1	0.9

tion 3.17). In order to calculate these fluxes additional parameters have to be specified. These parameters which are necessary for equation (3.12) are given in Tables 1 and 2. Figure 3 shows the comparison of measured and calculated values of F_{tv} again for the data of GOMES et al. (2003). Note that the physical dimensions of the horizontal and vertical flux components are different (kg m^{-1} s^{-1} in Figure 2, kg m^{-2} s^{-1} in Figure 3). Again the differences between simulated and measured fluxes are similar to those of GOMES et al. (2003). Here in most cases the differences are less than a factor of 5 but again for individual cases differences up to a factor of 10 are found. In case of the Niger data the binding energies e_i given in Table 1 had to be divided by a factor of 3 to obtain the agreement shown in Figure 3. This shows the necessity to adopt the parameter C and the binding energies to the local values, that means, when the parameterization is used in a three dimensional model, for each grid point. Since a lot of source areas on the global scale are located in very remote areas such data are not available at the moment. A comparison of Figure 2 and Figure 3 shows that in general the agreement for the saltation flux is better than for the vertical dust flux. Keeping in mind the complex processes between saltation and dust emission this behaviour could be expected.

4 3-D case studies

The above described source parameterization has then been incorporated into the full three-dimensional model KAMM/DRAIS/MADEdust. The source terms for number and mass concentrations are calculated from F_{tv} according to equations (3.1) and (3.2). Advection, diffusion and sedimentation are calculated from equations (2.1) and (2.2). As an application, we present a case study for the Dead Sea region. The Dead Sea is a saline lake in a narrow valley. Its surface lies 406 m below sea level. The lake is often covered by a haze layer. Mineral dust concentrations are often elevated in this region, due to local contributions and long-range transport from North Africa. SINGER et al. (2004) report dust loads up to 400 μg m^{-3} during individual dust storms in spring 2001, for which the particle size distribution indicated long-range transport. Singer et al. (2003) have analyzed mineral dust particles deposited during three years on a buoy in the Dead Sea. By their mineral composition, the

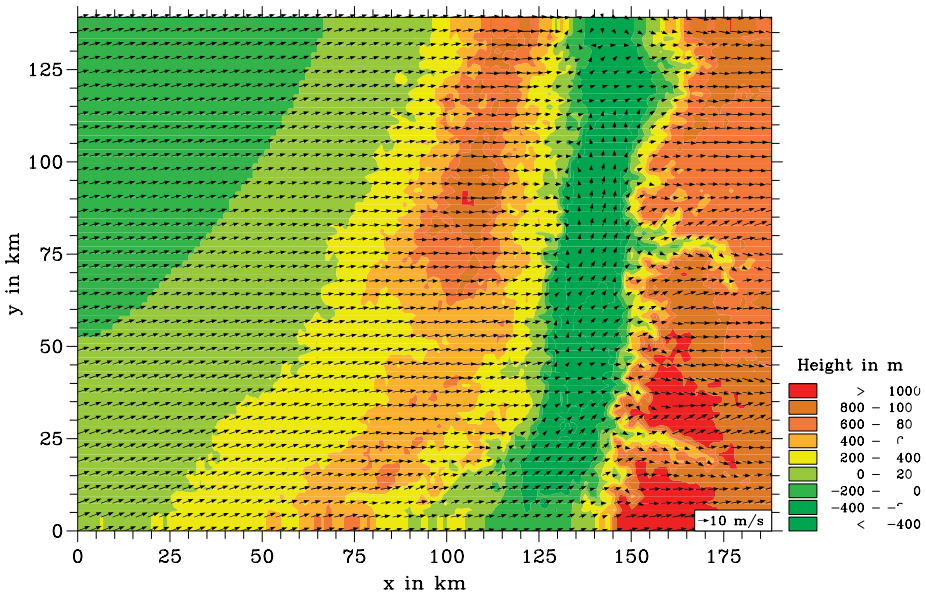

Figure 5: Horizontal wind at 20 m above ground at 3 p.m.

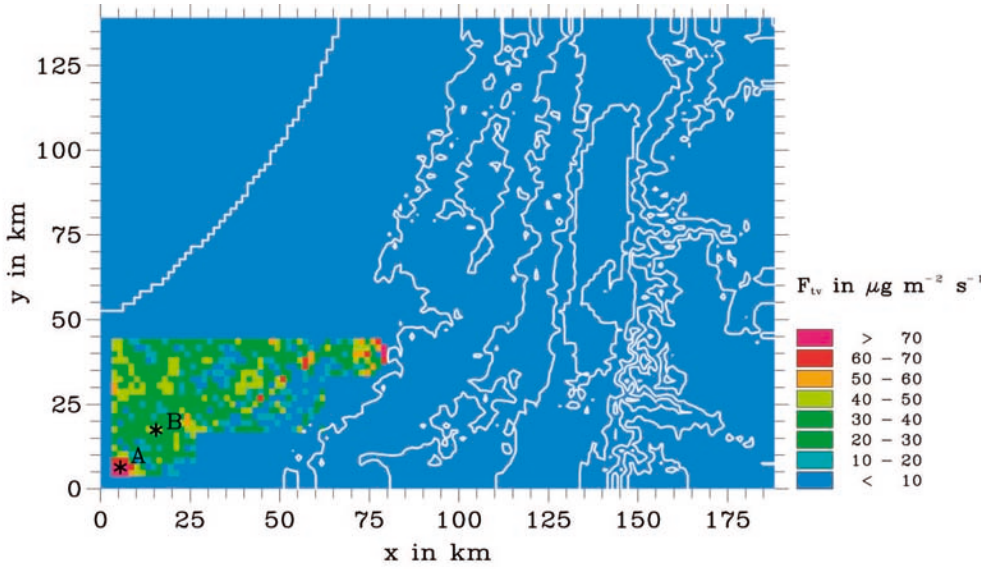

Figure 6: F_{tv} at 3 p.m.

Negev, Egyptian and Libyan deserts and Sinai could be identified as the particles' main source areas. TSIDULKO et al. (2002) used the model described in ALPERT et al. (2002) to simulate a dust storm in the eastern Mediterranean. For these simulations the horizontal grid spacing was 50 x 50 km^2. In order to resolve the Dead Sea on the model grid, a higher resolution is essential. This together with computing time restraints in turn limit the possible extensions of the model region.

4.1 Description of the model set-up

We therefore chose a region extending from 34E to 36E and from 30.75N to 32N over 190 x 141 km^2. The horizontal size of the grid cells is 1.58 x 1.88 km^2. 25 layers are used in the vertical direction. The vertical grid size varies between 20 m close to the surface and 500 m at the top of the model domain which is located 8 km above surface. The area covers the Dead Sea valley, part of the Mediterranean Sea, and the northern part of the Negev desert (see Figure 4). A sandy region in the Beersheba Depression in the western Negev and in the neighbouring Sinai was chosen as source area for mineral dust emission. Other parts of Negev where not used as source areas because they are mainly stony and our parameterization probably does not describe the emission processes in such environments appropriately. The rectilinear limits of the source area were roughly estimated from maps and are also depicted in Figure 4. Only 70 % of this area was admitted as effective sources. Emission was suppressed along the model boundaries to avoid re-

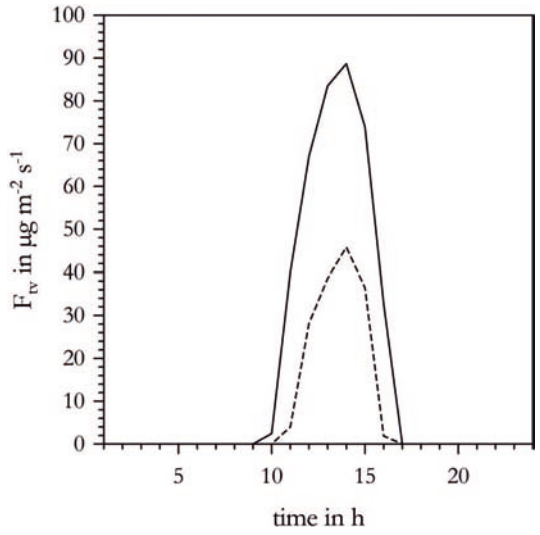

Figure 7: F_{tv} at points A (solid line) and B (dotted line) from Figure 6.

flection. To the extent of our knowledge, no other modelling studies have been undertaken for dust emission in this region. Therefore we had to resort to simplified assumptions about the parameters which enter the dust emission parameterization. For the soil particle size distribution, we used a typical Saharan soil (coarse medium sand) determined by CHATENET et al. (1996) (see Table 4). C (equation 3.7) is set to its original value of 2.61 and the binding energies given in Table 1 are used. The source area is attributed to the vegetation class "bare soil" with a roughness length z_0 (equation 3.5) of $2 \cdot 10^{-4}$ m.

The model has been run for 24 hours, but results have been analysed only from 9 a.m. to 12 p.m. For the large scale pressure field we assumed a western geostrophic wind (15 m s^{-1}) with a small southern component (1 m s^{-1}). ISRAELEVICH et al. (2003) studied the optical properties of dust particles over Israel based on TOMS und AERONET data. Although they found the dust sources to be located in North Africa they found westerly flow conditions for the situation in April. Radiation was specified for a day in the middle of April. Surface temperatures and start profiles were selected accordingly. From NCEP-reanalysis data (KALNAY et al., 1996) the surface temperature of the Mediterranean Sea was determined to typically 18° C, whereas the Dead Sea is already much warmer in this season (25° C). The initial surface temperature of bare soil is 17.5° C. A linear profile was assumed for the basic state of the potential temperature (22° C at ground level, 42° C at 6000 m above ground). These values correspond to long-year averages from NCEP reanalysis data for 35E, 31N. Relative humidity was assumed to vary linearly from 50 % at ground level to 10 % in 2000 m above ground and to remain constant above.

4.2 Model results

The distribution of the horizontal wind (Figure 5) shows a strong channelling effect in the Dead Sea valley. Figure 6 depicts the total vertical emission flux F_{tv} at 3 p.m. The strong variations within the source region are due to different values of u_*, while all soil parameters are constant over the whole area. The maximum emission strength in the south-western corner might be related to boundary effects. The source flux varies strongly with time, as can be seen in Figure 7 for two selected grid points. Point A represents a grid cell where the highest emission flux occurs while B represents moderate emission conditions. Dust is emitted from 9 a.m. to 5 p.m. at the point with higher total emission and at only from 10 p.m. to 5 p.m. at the second point. The proportions of the three dust modes vary during emission, as is intended by our parameterization. Still, the variations are rather small (Figure 8). The smallest mode which makes up only around 1 % in mass but around 80 % in number (not shown) has a maximum contribution at 2 p.m. The largest mode, on the other hand, behaves reciprocally and contributes most at the beginning and ending of the dust event, when u_* and therefore the kinetic energy of the saltation particles are smaller. During the emission period about 807 t of mineral dust are emitted.

The spatial and temporal distribution of the dust cloud is depicted in Figure 9. Maximum concentrations in vicinity of the source are above 435 μg m^{-3}. Concentrations in some distance still reach 116 μg m^{-3}. The colour scale on Figure 9 however has been chosen with respect to the following interesting feature. Transport of the dust is disturbed near the Dead Sea. At 3 p.m. a part of the dust cloud is redirected in a northern direction by the channelled winds. At 6 p.m. concentrations in the Dead Sea valley are still elevated. The cross section which is shown in Figure 10 shows the strong modification of the concentration distribution due to the topography. From model results not presented here we know that the Jordan Valley in the vicinity of the Death Sea causes a stable thermal stratification. This stable stratification is due to the subsidence inside the valley and the constant temperature of the Dead Sea during the course of the day. This stable stratification leads to a small vertical mixing and also supports the hypothesis that the topography hinders eastward transport. Size distributions in the source region at 12 a.m. and at the Dead Sea at 5 p.m. are finally shown in Figure 11. Sedimentation of the dust particles changes the size distributions of the number density and the mass density respectively. Since the total mass density decreases during the transport the size distributions were normalized by their maximum value in each case. While the total mass density at a typical gridpoint in the source area is 204 μg m^{-3} it decreases to 1 μg m^{-3} in the Dead Sea region.

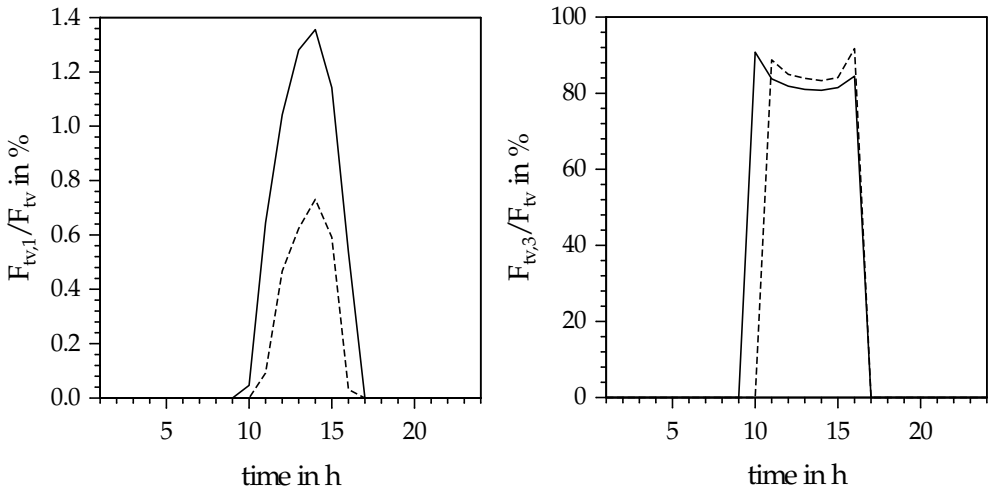

Figure 8: Proportions of the smallest (left) and largest mode (right) at points A (solid line) and B (dotted line).

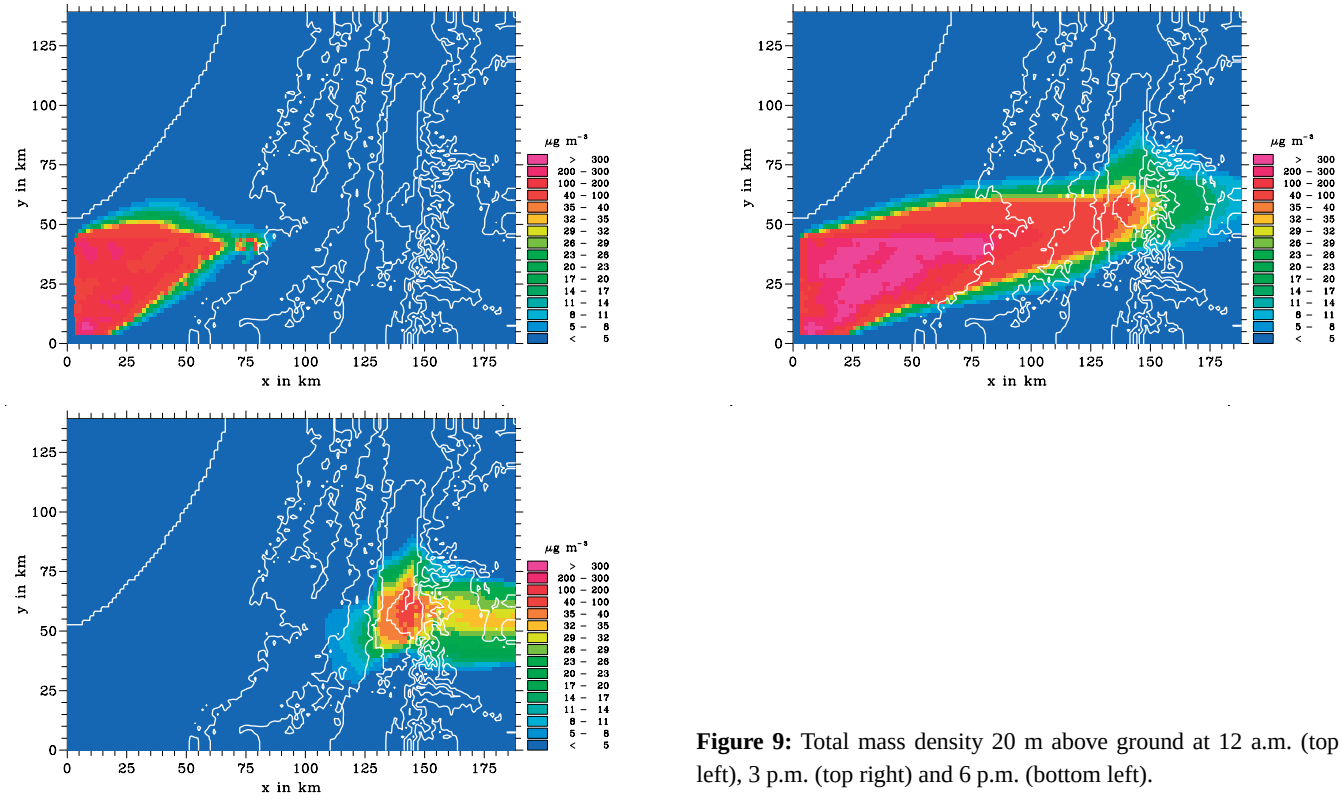

Figure 9: Total mass density 20 m above ground at 12 a.m. (top left), 3 p.m. (top right) and 6 p.m. (bottom left).

The effect of the size dependent sedimentation velocity is clearly shown. The relative contribution of larger particles to the total number density decreases at larger distances. This is an important effect with respect to the radiative effects of the particles and cannot be reproduced by a model that uses only one mode to represent the mineral dust particles. From our modelled size distributions we got a mass median diameter of 14 μm. OFFER and GOOSSENS (2004) carried out long term measurements in the Negev desert. They found median diameters around 25 μm or less. This shows that we underestimate the fraction of larger particles in the source area.

4.3 Comparison with other parameterizations and sensitivity study

As mentioned at the beginning there are several models documented in literature that treat the emission of airborne mineral dust particles. With respect to the emissions a lot of them are based on the parameterization of the saltation flux. The vertical emission flux is then often calculated using the following relation:

$$F_{tv} = \alpha \cdot F_{th} \tag{4.1}$$

In that case α has to be specified and is kept constant in time at each grid point. Then the total emission flux

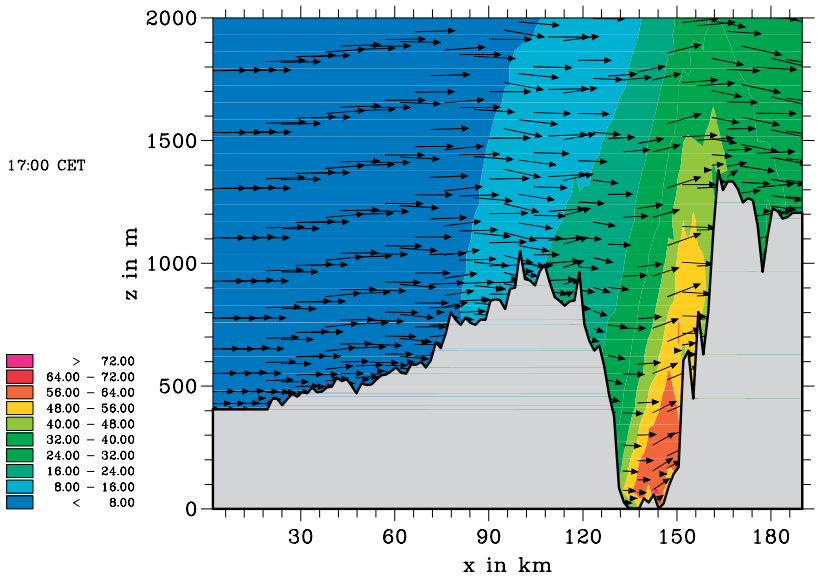

Figure 10: Vertical cross-section of mass density in μg m^{-3} at $y = 60$ km at 5 p.m.

is distributed to individual modes. For the individual modes the percentage contribution to F_{tv}, the median diameters and the standard deviations have to be prescribed. CAUTENET et al. (2000) distribute 0.1 % of F_{tv} to a 0.105 μm mode, 57.9 % to a 5 μm mode, and 42 % to a 35 μm mode. For the global model ECHAM5-HAM (STIER et al., 2005) fixed distributions to a 0.37 μm mode and a 1.75 μm mode are prescribed. TEGEN et al. (2002) are distributing the emission into 8 size classes ranging from 0.1 μm up to 220 μm. The percentage contribution of the total emission flux is not documented in the paper. The advantage of our parameterization is that neither α nor the percentage contribution of the individual modes to the total emissions is kept constant, but depends on the friction velocity and if the information is available on the water content of the soil. This will be shown in the following. Based on the results presented in Figure 6 and the corresponding saltation flux we calculated α at each grid point. Figure 12 shows the horizontal distribution of α and its frequency distribution. In that case α varies between 0 and $2.2 \cdot 10^{-5}$ m^{-1}.

In order to elucidate the variation of α we carried out simulations with the stand alone version of our emission module. We are using the same soil type and consequently the same parameters as we did in the Dead Sea case. The only difference is that the fraction of erodible surface is set equal to 100 %. Figure 13 shows the variation of α with u_*. When u_* is greater than a certain value α starts to increase reaching a maximum at $u_* = 0.44$ m s^{-1} and is then decreasing when the friction velocity is increasing. Most of the commonly used parameterizations use a constant value for α. For the source type we used for the sensitivity runs MARTICORENA et al. (1997) used $\alpha = 3.3 \cdot 10^{-5}$ m^{-1}. This causes large

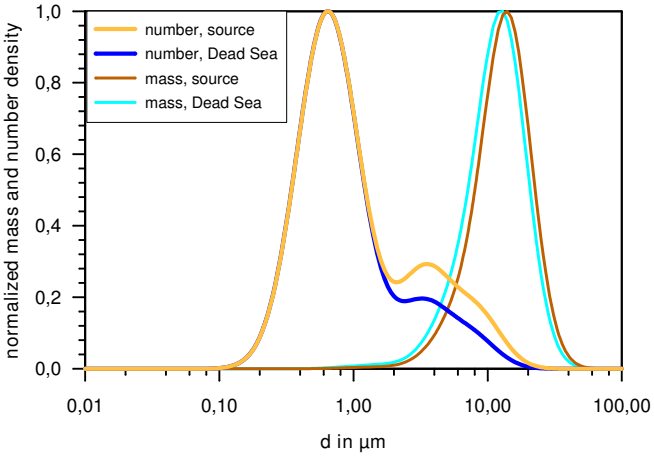

Figure 11: Normalized size distributions for number and mass density in the source region and the Dead Sea area.

differences in the emission flux compared to our parameterization. Especially, with the parameterization by MARTICORENA et al. (1997), the vertical dust emission starts immediately when the saltation flux is greater than zero. This is not the case for the parameterization we applied. The lower part of Figure 13 shows the vertical emission flux as a function of the friction velocity. The total flux and the percentage contribution of the individual modes are depicted. When the friction velocity is close to the threshold value the biggest mode contributes about 95 % to the total emission flux while the contribution of the finest mode is almost zero. At a friction velocity of 0.8 m s^{-1} the percentage contribution of the fines mode reaches almost 18 % of the total emission flux and the contribution of the biggest mode decreases down to 65 %. This behaviour seems to be quite reason-

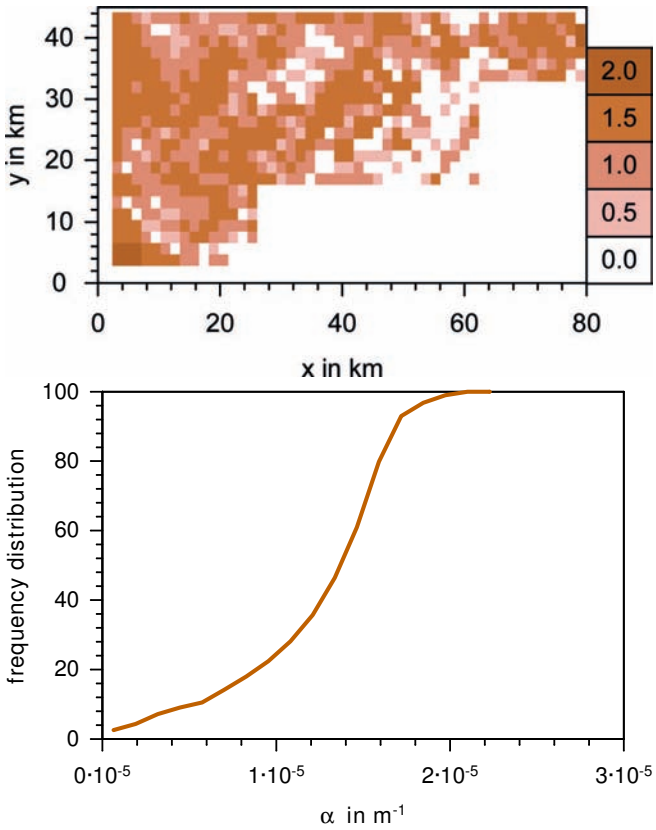

Figure 12: Horizontal distribution of α at 3 p.m. (top, values are given in 10^{-5} m^{-1}) and the corresponding frequency distribution (bottom).

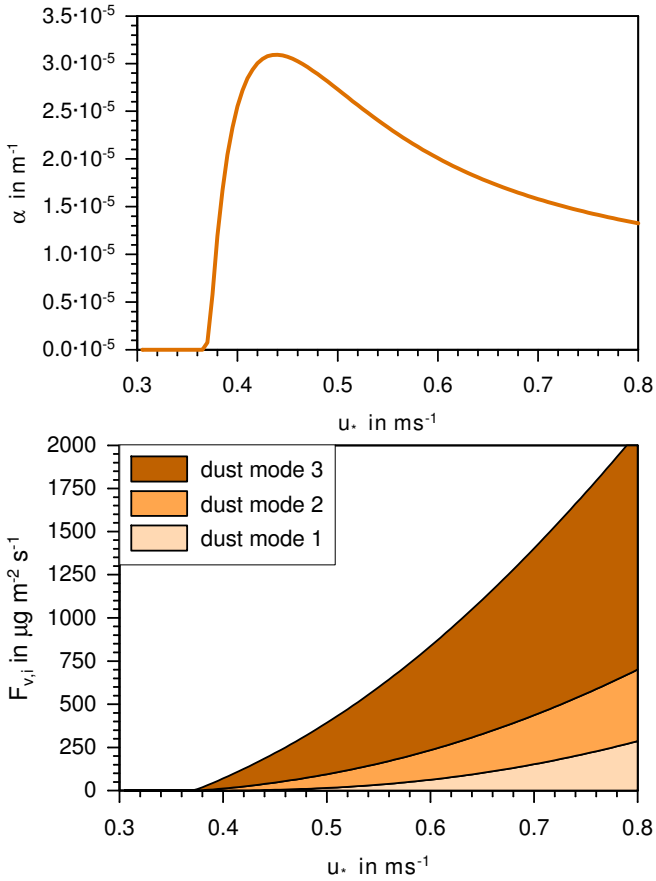

Figure 13: α (top) and the vertical emission flux (bottom) as a function of u_*.

able since the smallest particles have the highest binding energy.

In the case study described in section 4.1 we did not take into account the dependency of the emission flux on the soil water content. However, the parameterization we used in our study would allow such a dependency. Again we used the stand alone version of our emission model to present the effect of soil water content on the emission flux. Figure 14 shows α as a function of the soil water content η. In this case study we used a constant friction velocity of 0.4 m s^{-1}. In that case α decreases almost linearly with the soil water content and the emission stops when it reaches 5 %. The increasing soil water content goes along with a decreasing fraction of the finest particles to the total emission.

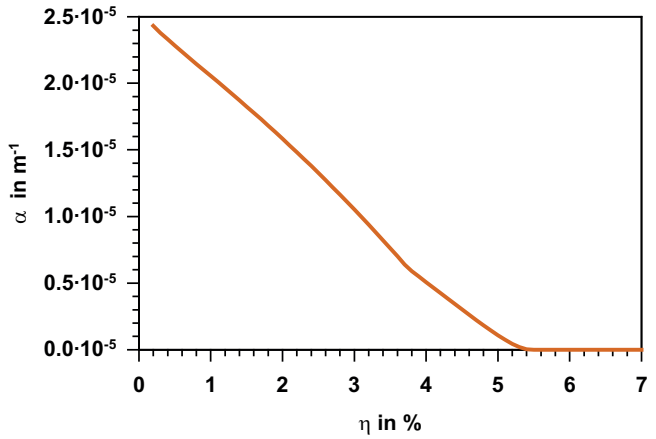

Figure 14: α versus the soil water content.

5 Summary

We have included a parameterization scheme of the emissions of dust particles in our regional scale model. It combines the parameterization of the threshold friction velocity of LU and SHAO (1999) and the parameterization of the saltation process of ALFARO and GOMES (2001). This parameterization was compared in a stand alone version to observed data of the saltation flux and the emission flux, respectively. As it was shown in other studies, some of the parameters had to be adjusted to obtain an optimal agreement. Nevertheless, in some cases big differences are found between the observed and the modelled fluxes. This shows that still experimental work is necessary to improve the currently used emission models for mineral dust particles. We included this parameterization into the three dimensional mesoscale model system KAMM/DRAIS/MADEsoot (RIEMER et al., 2003). The extended model system was applied to the Dead Sea area. It was shown that the complex mod-

ification of the flow field due to Jordan Valley has an impact on the distribution of the mineral dust particles. The model results show that the size distributions of the number and the mass density are modified by the size dependent sedimentation. This is an important aspect when the radiative effects of mineral dust particles are quantified. Finally we compared our parameterization with a very commonly used one. The advantage of our parameterization is that it allows a time dependent ratio of the saltation and the emission flux and a varying size distribution of emitted particles at each grid point which seems to be physically more reasonable. However, as for all parameterizations, it suffers from the lack of input data.

Acknowledgements

We want to thank S. ALFARO who gave us access to his calculations for the data measured in Spain and in Niger. We thank M. HANTEL for the thorough reading of our manuscript and his critical comments.

References

ACKERMANN, I. J., H. HASS, M. MEMMESHEIMER, A. EBEL, F. B. BINKOWSKI, U. SHANKAR, 1998: Modal Aerosol Dynamics Model for Europe: Development and first applications. – Atmos. Environ. **32**(17), 2981–2999.

ALFARO, S. C., L. GOMES, 1995: Improving the large-scale modeling of the saltation flux of soil particles in presence of nonerodible elements. – J. Geophys. Res. **100**(D8), 16357–16366.

ALFARO, S. C., L. GOMES, 2001: Modeling mineral aerosol production by wind erosion: Emission intensities and aerosol size distributions in source areas. – J. Geophys. Res. **106**(D16), 18075–18084.

ALPERT, P., KRICHAK, S.O., TSIDULKO, M., SHAFIR, H., JOSEPH, J.H., 2002: A dust prediction system with TOMS initialization. – Month. Wea. Rev. **130**, 2335–2345.

ANDREAE, M. O., 1996: Raising dust in the greenhouse. – Nature **380**, 389–390.

BAGNOLD, R. A., 1941: The Physics of Blown Sand and Desert Dunes. – Methuen & Co. Ltd., London.

BINKOWSKI, F. S., U. SHANKAR, 1995: The Regional Particulate Matter Model, 1. Model description and preliminary results. – J. Geophys. Res. **100**(D12), 26191–26209.

BISHOP, J. K. B., R. E. DAVIS, J. T. SHERMAN, 2002: Robotic observations of dust storm enhancement of carbon biomass in the north pacific. – Science **298**, 817–821.

CHATENET, B., B. MARTICORENA, L. GOMES, G. BERGAMETTI, 1996: Assessing the micro-ped size distributions of desert soils erodible by wind. – Sedimentology **43**, 901–911.

CAUTENET, G., F. GUILLARD, B. MARTICORENA, G. BERGAMETTI, F. DULAC, J. EDY, 2000: Modeling of a Saharan dust event. – Meteorol. Z. **9**, 221–230.

FÉCAN, F., B. MARTICORENA, G. BERGAMETTI, 1999: Parametrization of the increase of the aeolian erosion threshold wind friction velocity due to soil moisture for arid and semi-arid areas. – Annales Geophysicae **17**, 149–157.

GENTHON, C., 1992: Simulation of desert dust and sea-salt aerosols in Antarctica with a general circulation model of the atmosphere. – Tellus **44B**, 371–389.

GILLETTE, D. A., R. PASSI, 1988: Modeling dust emission caused by wind erosion. – J. Geophys. Res. **93**(D11), 14233–14242.

GINOUX, P., M. CHIN, I. TEGEN, J. M. PROSPERO, B. HOLBEN, O. DUBOVIK, S.-J. LIN, 2001: Sources and distributions of dust aerosols simulated with the GOCART model. – J. Geophys. Res. **106**(D17), 20255–20273.

GOMES, L., J. L. RAJOT, S. C. ALFARO, A. GAUDICHET, 2003: Validation of a dust production model from measurements performed in semi-arid agricultural areas of Spain and Niger. – Catena **52**, 257–271.

GONG, S. L., X. Y. ZHANG, T. L. ZHAO, I. G. MCKENDRY, D. A. JAFFE, N. M. LU, 2003: Characterization of soil dust aerosol in China and its transport and distribution during 2001 ACE-Asia: 2. Model simulation and validation. – J. Geophys. Res. **108**(D9), 4262, Doi:10.1029/2002JD002633.

GREELEY, R., J.D. IVERSEN, 1985: Wind as a Geological Process on Earth, Mars, Venus and Titan. – Cambridge University Press, New York, 333 pp.

GRIFFIN, D. W., C. A. KELLOG, V. H. GARRISON, J. T. LISLE, T. C. BORDEN, E. A. SHINN, 2003: Atmospheric microbiology in the northern Caribbean during African dust events. – Aerobiologia **19**, 143–157.

GRINI, A., C. S. ZENDER, 2004: Roles of saltation, sandblasting, and wind speed variability on mineral dust aerosol size distribution during the Puerto Rican Dust Experiment (PRIDE). – J. Geophys. Res. **109**(D7), D07202, Doi:10.1029/2003JD004233.

IN, H.-J., S.-U. PARK, 2002: A simulation of long-range transport of Yellow Sand observed in April 1998 in Korea. – Atmos. Environ. **36**, 4173–4187.

ISRAELEVICH, P. L., E. GANOR, Z. LEVIN, J. H. JOSEPH, 2003: Annual variations of physical properties of desert dust over Israel. – J. Geophys. Res. **108**(D13), 4381, Doi:10.1029/2002JD003163.

KALNAY, E., M. KANAMITSU, R. KISTLER, W. COLLINS, D. DEAVEN, L. GANDIN, M. IREDELL, S. SAHA, G. WHITE, J. WOOLLEN, Y. ZHU, A. LEETMAA, B. REYNOLDS, M. CHELLIAH, W. EBISUZAKI, W. HIGGINS, J. JANOWIAK, K. C. MO, C. ROPELEWSKI, J. WANG, R. JENNE, D. JOSEPH, 1996: The NCEP/NCAR 40-Year Reanalysis Project. – Bull. Amer. Meteor. Soc. **77**(3), 437-471.

LEVIN, Z., E. GANOR, V. GLADSTEIN, 1996: The Effects of Desert Particles Coated with Sulfate on Rain Formation in the Eastern Mediterranean. – J. Appl. Meteor. **35**, 1511–1523.

LU, H., Y. SHAO, 1999: A new model for dust emission by saltation bombardment. – J. Geophys. Res. **104**(D14), 16827–16841.

LU, H., Y. SHAO, 2001: Toward quantitative prediction of dust storm: an integrated wind erosion modelling system and its applications. – Environ. Modelling and Software **16**, 233–249.

MARTICORENA, B., G. BERGAMETTI, 1995: Modeling the atmospheric dust cycle: 1. Design of a soil-derived dust emission scheme. – J. Geophys. Res. **100**(D8), 16415–16430.

MARTICORENA, B., G. BERGAMETTI, B. AUMONT, Y. CALLOT, C. N'DOUMÉ, M. LEGRAND, 1997: Modeling the atmospheric dust cycle: 2. Simulation of Saharan dust sources. – J. Geophys. Res. **102**(D4), 4387–4404.

MILLER, R. L., I. TEGEN, J. PERLWITZ, 2004: Surface radiative forcing by soil dust aerosols and the hydrological cycle. – J. Geophys. Res. **109**, D04203, Doi:10.1029/2003JD004085.

NICKOVIC, S., G. KALLOS, A. PAPADOPOULOS, O. KAKALIAGOU, 2001: A model for prediction of desert dust cycle in the atmosphere. – J. Geophys. Res. **106**(D16), 18113–18129.

OFFER, Z.Y., D. J. GOOSSENS, 2004: Thirteen years of aeolian dust dynamics in a desert region (Negev desert, Israel): Analysis of horizontal and vertical dust flux, vertical dust distribution and dust grain size. – Arid Environ. **57**, 117–140.

OWEN, P. R., 1964: Saltation of uniform grains in air. – J. Fluid Mech. **20**(2), 225–242.

RIEMER, N., H. VOGEL, B. VOGEL, F. FIEDLER, 2003: Modeling aerosols on the mesoscale-γ: Treatment of soot aerosol and its radiative effects. – J. Geophys. Res. **108**(D19), 4601, Doi:10.1029/2003JD003448.

ROSENFELD, D., Y. RUDICH, R. LAHAV, 2001: Desert dust suppressing precipitation: A possible desertification feedback loop. – Proceedings of the National Academy of Science **98**(11), 5975–5980.

SCHELL, B., I. J. ACKERMANN, H. HASS, F. S. BINKOWSKI, A. EBEL, 2001: Modeling the formation of secondary organic aerosol within a comprehensive air quality model system. – J. Geophys. Res. **106**(D22), 28,275–28,294.

SCHÖNFELDT, H.-J., 2004: Establishing the threshold for intermittent aeolian sediment transport. – Meteorol. Z. **13**, 437–444.

SCHÖNFELDT, H.-J., S. VON LOEWIS, 2003: Turbulence-driven saltation in the atmospheric surface layer. – Meteorol. Z. **12**, 257–268.

SEINFELD, J. H., S. PANDIS, 1998: Atmospheric Chemistry and Physics. – John Wiley & Sons, Inc., 1326 pp.

SHAO, Y., 2000: Physics and Modelling of Wind Erosion. – Vol. 23 of Atmospheric and Oceanographic Sciences Library, Kluwer Academic Publishers, Dordrecht, Netherlands.

—, 2001: A model for mineral dust emission. – J. Geophys. Res. **106**(D17), 20239–20254.

SHAO, Y., H. LU, 2000: A simple expression for wind erosion threshold friction velocity. – J. Geophys. Res. **105**(D17), 22437–22443.

SINGER, A., E. GANOR, S. DULTZ, W. FISCHER, 2003: Dust depostition over the Dead Sea. – J. Arid Environ. **53**, 41–59, Doi:10.1006/jare.2002.1023.

SINGER, A., S. DULTZ, E. ARGAMAN, 2004: Properties of the non-soluble fractions of suspended dust over the Dead Sea. – Atmos. Environ. **38**, 1745–1753.

SONG, Z., 2004: A numerical simulation of dust storms in China. – Environ. Modelling and Software **19**, 141–151.

STIER, P., J. FEICHTER, S. KINNE, S. KLOSTER, E. VIGNATI, J. WILSON, L.GANZEVELD, I. TEGEN, M. WENER, Y. BALKANSKI, M. SCHULZ, O. BOUCHER, 2005: The aerosol-climate model ECHAM5-HAM. – Atmos. Chem. Phys. **5**, 1125–1156.

TEGEN, I., 2003: Modeling the mineral dust aerosol cycle in the climate system. – Quaternary Science Rev. **22**, 1821–1834.

TEGEN, I., I. FUNG, 1994: Modelling of mineral dust in the atmosphere: Sources, transport, and optical thickness. – J. Geophys. Res. **99**(D11), 22897– 22914.

TEGEN, I., S. P. HARRISON, K. E. KOHFELD, I. C. PRENTICE, M. C. COE, M. HEIMANN, 2002: The impact of vegetation and preferential source areas on global dust aerosol: Results from a model study. – J. Geophys. Res. **107**, 4576, Doi:10.1029/2001JD000963.

TSIDULKO, M., S. O. KRICHAK, P. ALPERT, O. KAKALIAGOU, G. KALLOS, A. PAPADOPOULOS, 2002: Numerical study of a very intensive eastern Mediterranean dust storm, 13-16 March 1998. – J. Geophys. Res. **107**(D21), 4581, Doi:10.1029/2001JD001168.

VOGEL, B., F. FIEDLER, H. VOGEL, 1995: Influence of topography and biogenic volatile organic compounds emission in the state of Baden-Württemberg on ozone concentrations during episodes of high air temperatures. – J. Geophys. Res. **100**(D11), 22907–22928.

WHITE, B. R., 1979: Soil transport by winds on Mars. – J. Geophys. Res. **84**, 4643–4651.

ZENDER, C. S., R. L. MILLER, I. TEGEN, 2004: Quantifying mineral dust mass budgets: Systematic terminology, constraints, and current estimates. – Eos **85**, 509–512.